Characterizing cell-type spatial relationships across length scales in spatially resolved omics data

Rafael dos Santos Peixoto[1,2], Brendan F. Miller[1,2], Maigan A. Brusko[3], Gohta Aihara[1,2], Lyla Atta[1,2], Manjari Anant[1,4], Mark A. Atkinson[3], Todd M. Brusko[3], Clive H. Wasserfall[3], Jean Fan[1,2]

[1] Center for Computational Biology, Whiting School of Engineering, Johns Hopkins University, Baltimore, MD 21211

[2] Department of Biomedical Engineering, Johns Hopkins University, Baltimore, MD 21218,

[3] Department of Pathology, Immunology, and Laboratory Medicine, University of Florida, Gainesville, FL 32610

[4] Department of Neuroscience, Johns Hopkins University, Baltimore, MD 21205

Correspondence should be addressed to:

Jean Fan (jeanfan@jhu.edu)

Key words: spatial omics, single cell, colocalization, spatial relationships, spatial subsetting

Abstract

Spatially resolved omics (SRO) technologies enable the identification of cell types while preserving their organization within tissues. Application of such technologies offers the opportunity to delineate cell-type spatial relationships, particularly across different length scales, and enhance our understanding of tissue organization and function. To quantify such multi-scale cell-type spatial relationships, we developed CRAWDAD, Cell-type Relationship Analysis Workflow Done Across Distances, as an open-source R package with source code and additional documentation at https://jef.works/CRAWDAD/.

To demonstrate the utility of such multi-scale characterization, recapitulate expected cell-type spatial relationships, and evaluate against other cell-type spatial analyses, we applied CRAWDAD to various simulated and real SRO datasets of diverse tissues assayed by diverse SRO technologies. We further demonstrate how such multi-scale characterization enabled by CRAWDAD can be used to compare cell-type spatial relationships across multiple samples. Finally, we applied CRAWDAD to SRO datasets of the human spleen to identify consistent as well as patient and sample-specific cell-type spatial relationships. In general, we anticipate such multi-scale analysis of SRO data enabled by CRAWDAD will provide useful quantitative metrics to facilitate the identification, characterization, and comparison of cell-type spatial relationships across axes of interest.

Introduction

Spatially resolved omics (SRO) technologies enable molecular profiling to facilitate the identification of distinct cell types while preserving their spatial organization within tissues, providing an opportunity to evaluate cell-type spatial relationships. Cell-type spatial relationships

such as colocalizations, defined as which cell types are spatially near each other, and separations, defined as which cell types are spatially away from each other, may exhibit distinct trends relevant to healthy tissue function[1] as well as disease[2]. As such, evaluating these cell-type spatial relationships provide an opportunity to advance our understanding of the association between cell-type organization, tissue function, and disease.

Cell-type spatial relationships can occur at different length scales, with some cell types colocalizing to engage in paracrine signaling and other close-range interactions at a fine, micrometer length scale[3]; others colocalizing into distinct environments and functional tissue units at a more meso-scale[1]; while others colocalizing into anatomical structures at a more macro-scale (Fig 1a-b). Whether we consider two cell-types as being colocalized is often a function of the spatial extent that we analyze (Fig 1b). For example, two cell types uniquely present in distinct layers of the brain may be considered separated if we consider only the spatial extent of the brain. However, we may consider these cell types to be colocalized in the same organ if we consider the spatial extent of the whole body. Thus, we sought to consider the effects of spatial extent by investigating cell-type spatial relationships across different length scales.

To quantitatively evaluate such cell-type spatial relationships across length scales, we present CRAWDAD, Cell-type Relationship Analysis Workflow Done Across Distances. We demonstrate CRAWDAD on simulated as well as real SRO datasets for diverse tissues assayed by seqFISH[4], Slide-seqV2[5], Xenium[6], MERFISH[7], and CODEX[8], though CRAWDAD is amenable to any SRO data for which cell positions and cell-type annotations can be obtained. CRAWDAD is available as an open-source R package at https://github.com/JEFworks-Lab/CRAWDAD with additional documentation and tutorials available at https://jef.works/CRAWDAD/.

Results

<u>Overview of Method</u>

Given cell centroid positions and their cell-type annotations, CRAWDAD evaluates the statistical enrichment or depletion of each cell-type within the spatial neighborhood around cells of a reference cell-type at a particular spatial length scale. To achieve this, CRAWDAD first draws a neighborhood around cells of a reference cell type based on a user-defined neighborhood distance d and calculates the proportion of every cell type inside the neighborhood of this reference cell type, excluding the original reference cell that seeded the neighborhood (Fig 1c). Next, CRAWDAD creates a series of non-overlapping grids of tiles (square or hexagonal) where the side-length of each tile corresponds to a user-defined spatial length scale. Then, it shuffles the cell-type annotations for all cells within each tile to create an empirical null background at the specified spatial length scale (Fig 1d). Lastly, given the observed and shuffled cell-type annotations, CRAWDAD uses a binomial proportion testing framework to evaluate if the observed cell-type proportions are significantly different from what is expected by chance based on the shuffled data. In this process, we obtain a Z-score for each neighbor and reference cell-type pair at the given spatial length scale. To assess statistical significance, we use default Z-scores of ±1.96 (p-value = 0.05) with multiple testing correction based on the number of cell-type combinations evaluated. For a given cell-type pair, if their Z-score is above the positive significance threshold, we interpret the neighbor cell type as being enriched in the neighborhood of the reference cell type; if their Z-score is below the negative significance threshold, we interpret the neighbor cell type as being depleted in the neighborhood of the reference cell type. In addition, we define colocalization as the mutual enrichment of cell types within each other's neighborhoods. Alternatively, we define separation as the mutual depletion of the cell types within each other's neighborhoods.

To evaluate spatial relationships with different spatial extents, CRAWDAD repeats this process for a series of spatial length scales. In this manner, we obtain a Z-score for each cell-type pair in each spatial length scale. We can visualize the results by plotting the Z-scores on the y-axis and the length scales on the x-axis, creating a multi-scale spatial relationship trend plot for each cell-type pair. Here, we refer to the scale of the relationship between two cell-types as the first evaluated spatial length scale in which the Z-score is above the significance threshold. To summarize spatial relationships across all cell-type pairs, we plot the scale of the relationships and associated Z-scores as a dot plot. To mitigate grid edge effects, CRAWDAD uses different random seeds and grid offsets to create multiple permutations of the shuffled data. The Z-scores obtained for each cell-type pair at each length scale are then averaged across permutations.

CRAWDAD characterizes cell-type spatial relationships at multiple length scales in simulated data

To highlight the utility of evaluating cell-type spatial relationships across multiple length scales, we first simulated 8,000 cells representing four cell types in a 2000μm-by-2000μm tissue sample (Methods). In this simulated dataset, cell-types B and C are spatially intermixed with one another, while cell-type A forms a distinct structure around cell-types B and C, that further isolate them from cell-type D (Fig 1b). We applied CRAWDAD to characterize the spatial relationships between each cell-type pair across length scales ranging from 100μm to 1000μm using a neighborhood size of 50μm (Methods). We found that the neighborhood around reference cell-type C is significantly enriched with cells of cell-type B from a fine length scale of ~150μm (Fig 1e,g). Likewise, we observed that the neighborhood around reference cell-type B is significantly enriched with cells of cell-type C from a similarly fine length scale (Supp Fig 1a). Given this mutual enrichment relationship, we interpret cell-types B and C to be spatially colocalized from

this fine length scale. In contrast, we noted cell-types A and B to be spatially colocalized from a comparably coarser length scale of ~800μm (Fig 1f-g, Supp Fig 1b).

We note that some multi-scale cell-type spatial relationship trends will exhibit a monotonic behavior, tending towards only enrichment or depletion, while others might oscillate between enrichment and depletion. For example, the neighborhood around reference cell-type C exhibits an increasing Z-score with respect to neighbor cell-type B across length scales, resulting in a monotonically increasing spatial trend towards enrichment (Fig 1e). In contrast, the neighborhood around reference cell-type A exhibits an initially decreasing Z-score with respect to neighbor cell-type B that eventually becomes a positive Z-score at larger length scales, resulting in an oscillatory spatial trend (Fig 1f). Such an oscillatory spatial trend better reflects how cell-types A and B are separated in different compartments but ultimately comprise the same structures evident only at larger spatial extents. Other methods that evaluate spatial relationships only at the whole tissue scale may miss these distinctions regarding monotonic and oscillatory spatial trends. For example, Squidpy's neighborhood enrichment implementation of the approach described by Schapiro *et al.*[9] calculates an enrichment score based on the proximity of cell types from a spatial neighborhood graph created using a fixed distance[10]. Therefore, it does not capture the dynamics of such cell-type spatial relationships (Supp Fig 1c).

CRAWDAD's quantified cell-type spatial relationships are also robust as the spatial extent is broadened to a larger tissue section inclusive of new cell types. To demonstrate this, we expanded the tissue in the simulated data to include another cell type, cell-type E, not present in the original tissue (Supp Fig 1d). When we apply CRAWDAD to this expanded tissue, the spatial relationships for cell-types A, B, and C in terms of the quantified Z-scores remain the same (Fig 1e, Supp Fig 1f). In this manner, the spatial relationships for cell-types A, B, and C are robust to

the addition of the new cell type in expanded regions not considered in the original analysis. In contrast, when we apply Squidpy's neighborhood enrichment implementation to the original versus the expanded tissue, the neighborhood enrichment metrics for cell-types A, B, and C are altered (Supp Fig 1c, e).

To further benchmark and compare CRAWDAD's functionality, we simulated a variety of SRO datasets using a previously developed simulation framework[11] (Methods). Briefly, we simulated cells by sampling from a uniform distribution to create x-y positions. We split the cells into two groups, and, for each group, we associated a value to each cell using independent, autocorrelated Gaussian random fields (Supp Fig 2a). We binarized the values, splitting the cells into two cell-types based on the underlying simulated value (Supp Fig 2b). In this manner, we created a simulated dataset with four cell types (Supp Fig 2c) where we expect each cell-type to be enriched with itself due our use of spatially autocorrelated simulation values. Likewise, we can expect the two cell-types simulated from the same Gaussian random field to be spatially mutually exclusive and therefore identified to be separated. Additionally, we expect the cell-types from different random fields to exhibit no significant spatial relationship due to the Gaussian random fields being independent. We repeated this process to create a total of ten random simulated datasets.

We used these simulated datasets to benchmark and compare CRAWDAD with two other spatial relationship analysis methods that also consider spatial length scales, Ripley's K Cross[12] and Squidpy's co-occurrence implementation of the approach described in Tosti *et al.*[13] Although all evaluated methods perform cell-type enrichment analysis across length scales, their definition of length scales differs. Briefly, Ripley's K Cross evaluates multiple length scales by increasing the neighborhood size while comparing the cell-type proportion in the neighborhood to the global

proportion. On the other hand, Squidpy's co-occurrence implementation evaluates multiple length scales by increasing the size of an annulus neighborhood and calculating the conditional probability of the neighbor cell types given the reference cell type. In addition, as Ripley's K Cross and Squidpy's co-occurrence implementation do not present a threshold to determine statistical significance, for comparative purposes, we opted to assess each method's ability to distinguish between cell-type spatial enrichment and depletion. Specifically, given a reference cell type, we considered a method as achieving a true positive prediction if the cell type identified with the most enriched relationship trend was itself. Alternatively, we also considered a method as achieving a true positive prediction if the cell type identified with the most depleted relationship trend was the other cell type from the same Gaussian random field. We identified the cell-type with the most enriched and most depleted spatial trend using their area under the trend curve value (Methods). Using this approach, we evaluated all four cell types across all ten simulated datasets using all three methods (Supp Fig 2d). Based on this simulation framework, we obtained a true positive rate of 0.95 for CRAWDAD, 0.86 for Squidpy's co-occurrence implementation, and 0.8 for Ripley's K Cross. In this manner, cell-type spatial relationships identified by CRAWDAD can more accurately distinguish between cell-type spatial enrichment and depletion compared to other evaluated methods based on simulated data.

CRAWDAD recapitulates expected cell-type spatial relationships in the real spatial omics datasets of tissues

We next applied CRAWDAD to evaluate cell-type spatial relationships in SRO datasets of real tissues. First, we analyzed a spatial transcriptomics dataset obtained from a highly spatially organized tissue, the mouse cerebellum, assayed by Slide-seqV2[5] and previously annotated by

RCTD[14] (Fig 2a). Because Slide-seqV2 uses 10μm barcoded beads to profile the gene expression within tissues in a spatially resolved manner, spatially resolved measurements may not necessarily correspond to single cells. However, given that a typical animal cell is also roughly 10-20μm in size[15], we assumed here that the observed spatial position and cell-type assignments associated with each bead generally reflects the spatial position and cell-type annotations of the cell within the immediate vicinity of that bead. As such, we treat Slide-seqV2 beads with non-doublet RCTD annotations as effectively single cells for CRAWDAD analysis. We applied CRAWDAD to evaluate 10,098 annotated cells representing 19 cell-types using a neighborhood size of 50μm across length scales ranging from 100μm to 1000μm (Fig 2b, Methods). Among the significantly colocalized cell-type pairs identified were Purkinje neurons and Bergmann glia (Fig 2b-c, Supp Fig 3a), which are known to interact at close distances within the Purkinje cell layer of the cerebellum[16]. Likewise, the neighborhood around Purkinje neurons was significantly depleted of oligodendrocytes and vice versa (Fig 2b-c, Supp Fig 3b). As such, we may interpret these cell-types as being spatially separated, consistent with the known spatially distinct layer structure of the cerebellum. Additionally, we applied Ripley's K Cross (Fig 2d) and Squidpy's co-occurrence implementation (Fig 2e) to the same dataset. We find that these other methods do not as clearly distinguish these expected cell-type spatial relationships. Specifically, when analyzing cell-type spatial relationships with Purkinje neurons as the reference cell-type, we note that CRAWDAD's Z-score trend for Bergmann glia increases as the length scale increases, crossing the upper significance threshold and defining an enrichment of Bergmann glia among the neighborhood of Purkinje neurons as expected (Fig 2c). Likewise, CRAWDAD's Z-score trend for oligodendrocytes decreases as the length scale increases, crossing the lower significance threshold and defining a depletion of oligodendrocytes among the neighborhood of Purkinje neurons as

expected (Fig 2c). These two cell-type trends are further distinct from other cell-types in the cerebellum. This clear separation between these two cell-type trends is not observed in the other evaluated spatial analysis methods (Fig 2d-e).

Next, we analyzed a single-cell resolution spatial transcriptomics dataset of a whole developing embryo assayed by seqFISH[4] (Fig 2f). We applied CRAWDAD to evaluate cell-type spatial relationships for 19,416 cells representing 22 cell types using a neighborhood size of 50μm across length scales ranging from 100μm to 1000μm (Fig 2g, Methods). Consistent with the original publication's observations, CRAWDAD identified significant spatial colocalization between the intermediate and lateral plate mesoderm cells and significant spatial separation between intermediate plate mesoderm and cardiomyocyte cells (Fig 2g-h, Supp Fig 3c-d). Again, such differences between cell-type spatial relationships are difficult to discern using on other evaluated spatial analysis methods (Fig 2i-j).

To further exemplify CRAWDAD's applicability to potentially less well-organized tissues such as cancer tissues, we applied it to a breast cancer dataset assayed by Xenium[6] (Fig 3a). We applied CRAWDAD to evaluate 162,107 annotated cells representing 19 cell-types using a neighborhood size of 100μm across length scales ranging from 100μm to 1000μm (Fig 3, Methods). CRAWDAD identified three groups of cell types based on their cell-type spatial relationships, corresponding to histologically distinct structures (Fig 3b-e).

In general, we note that the cell-type spatial relationships identified in CRAWDAD are not always symmetric. Asymmetric results may be caused by two scenarios: location imbalance and density imbalance. In location imbalance, cells of the neighboring cell-type may be close to only some cells of the reference cell-type, but not all. For example, the neighborhood of UBCs is enriched with granule cells (Supp Fig 4a, c). However, UBCs are rare and present in only a small

proportion of the granule cells' neighborhood and therefore does not represent a significant relationship (Supp Fig 4b, d). In density imbalance, cells from one type are highly concentrated in one region, with a few dispersed across other parts of the tissue. Therefore, the sparse cells will contribute to the creation of the neighborhood as the reference cell type but will not significantly contribute to the proportions as the neighbor cell type, due to their small number. For example, a large part of the presomitic mesoderm's neighborhood is created by its sparse cells, which encapsulate spinal cord cells, creating a relationship of enrichment (Supp Fig 4e, g). On the other hand, most of the presomitic mesoderm cells are outside the spinal cord's neighborhood creating a relationship of depletion (Supp Fig 4f, h). Such asymmetric cell-type spatial relationships may reflect non-exclusive cell-type interactions. For example, immune cells may infiltrate a focal tumor such that the neighborhood of tumor cells will be enriched with immune cells, but the neighborhood of immune cells might not be enriched by tumor cells given their widespread spatial distribution throughout the body, consistent with a non-exclusive cell-type spatial relationship at a whole-body spatial extent[17]. Therefore, CRAWDAD can quantitatively capture such asymmetric cell-type spatial relationships and effectively delineate cell-type spatial relationships across multiple length scales for diverse tissues and SRO technologies.

CRAWDAD enables comparison of cell-type spatial relationships across multiple samples

Beyond characterizing cell-type spatial relationships within a single sample, such multi-scale characterization enabled by CRAWDAD can also be used to compare cell-type spatial relationships across samples spanning different conditions, such as health and disease, development, or replicates. To demonstrate this functionality, we applied CRAWDAD to nine mouse brain samples assayed by MERFISH comprised of three replicates from three distinct

Bregma locations[7] with cell-type annotations obtained previously using unified clustering[18] (Fig 4a). We applied CRAWDAD to evaluate 734,693 annotated cells across all datasets representing 14 cell-types using a neighborhood size of 50μm across length scales ranging from 100μm to 1000μm (Methods). To compare multi-scale cell-type spatial relationships across samples, we calculated the signed area under the curve (AUC) for each Z-score trend for each cell-type pair. We then performed dimensionality reduction with principal component analysis (PCA) on all signed AUC values to find that cell-type spatial relationships of replicates from the same Bregma location are highly similar, as they are positioned closer together in PC space (Fig 4b). We likewise overall observed a smaller variance in the signed AUC values within replicates from the same Bregma location compared to across locations (Fig 4c). These results suggests that samples from the same Bregma location have cell-type spatial relationships that are more similar than those from different Bregma locations, as expected. Importantly, this similarity in cell-type spatial relationships is robust to tissue rotation and small local diffeomorphisms, as some of the brain tissue sections profiled are rotated with small tissue distortions compared to others. To investigate specific highly variable cell-type spatial relationships further, we visualized the spatial-relationship trends for the cell-type pair with the highest signed AUC variance across locations: GABAergic Estrogen-Receptive Neurons as reference and Excitatory Neurons as neighbor (Fig 4d). Despite its comparatively higher signed AUC variance across locations, samples from the same Bregma location still generally exhibited the same depletion trend whereas samples across Bregma locations varied (Fig 4d). Visual inspection of GABAergic Estrogen-Receptive Neurons and Excitatory Neurons also suggested high consistency in terms of spatial relationships within replicates from the same Bregma location compared to across locations (Fig 4e). As such, cell-type spatial relationship trends quantified by CRAWDAD can be used to compare across samples

to confirm that cell-type spatial relationships in the mouse brain are generally highly consistent within replicates from the same Bregma location compared to across locations.

CRAWDAD reveals functionally relevant cell-type spatial relationships in the human spleen

Finally, we sought to apply CRAWDAD to characterize and compare cell-type spatial relationships in SRO datasets of the human spleen. The spleen is a highly structured organ where cell types interact to filter blood and initiate immune responses. Delineating the spatial organization of cell types in the spleen can provide insights into how these different cellular populations may achieve such diverse immunologic functions. Therefore, we focused on six single-cell resolution spatial proteomics datasets of the human spleen comprised of two replicates from three individuals each assayed by CODEX[8] as part of The Human BioMolecular Atlas Program (HuBMAP)[19]. We first performed graph-based clustering for one representative section of a human spleen with 154,446 cells to identify 12 cell types based on 28 protein markers (Figure 5a-c, Methods). Applying CRAWDAD with a neighborhood of 50μm and length scales ranging from 100μm to 1750μm, we observe cell-type spatial relationships to broadly recapitulate known splenic architecture. Cell-types primarily colocalized at a coarse length scale into two major compartments defined by follicle B cells and red pulp B cells corresponding to the white pulp (WP) and red pulp (RP), respectively[20] (Fig 5d). Consistent with the functional roles of these compartments, cell types identified to colocalize with red pulp B cells include macrophages, neutrophils, and monocytes that may remove old and dead red blood cells within the RP[21]. Likewise, cell types identified to colocalize with follicle B cells include CD4+ memory T cells and podoplanin-expressing cells within the WP (Fig 5d). Podoplanin-expression has been

previously associated with T-cell zone reticular cells[22] and observed to surround large arteries[23] within the WP.

To determine whether such cell-type spatial colocalization relationships are consistent across tissue sections and individuals, we further repeated these analyses with 837,952 cells from five additional spleen samples both within and across individuals. To ensure all datasets were annotated in a uniform manner, we applied batch-correction[24] and used a linear discriminant analysis model to transfer cell-type annotations to these new datasets (Methods, Supp Fig 5). We then applied CRAWDAD to identify similar cell-type spatial relationships corresponding to the WP and RP compartments both within and across individuals (Fig 5d, Supp Fig 6a). Further analyzing the variance of the relationship trend's AUC values (Fig 5e), we noticed that most cell-type spatial relationship trends were highly consistent across patients and samples, reflecting the ordered patterning of the functional tissue regions (Fig 5e-f, Supp Fig 7a). Select cell-type spatial relationship trends had patient-specific relationships, exhibiting consistent trends within replicates from the same patient but varying across patients, suggestive of potential patient-specific variation (Fig 5g, Supp Fig 7b). Other cell-type spatial relationship trends varied even within replicates, suggestive of potential tissue sample-specific patterns (Fig 5h, Supp Fig 7c). In general, we anticipate assessing these variations in cell spatial relationships can give insight into inter- and intra-individual variation linked to donor and tissue-specific features.

Although our clustering analysis identified a cluster of cells highly expressing CD4 and CD45RO proteins, which we interpreted as CD4+ memory T cells, we were unable to distinguish follicular helper T cells, a specialized subset of CD4+ memory T cells that play a critical role in the adaptive immune response, due to limitations of our 28 protein-marker panel. However, we know that follicular helper T cells interact with B cells during the B cell maturation and

differentiation process within the B cell follicles. As such, we hypothesized that follicular helper T cells would represent a spatially-defined subset of these CD4+ memory T cells that are colocalized with follicular B cells[25]. To identify putative follicular helper T cells, we therefore applied the same binomial testing framework used in CRAWDAD's pairwise spatial relationship testing to identify CD4+ memory T cells that are statistically enriched around follicle B cells (Fig 5i, Supp Fig 6b, Methods). Briefly, for each given cell, we perform an exact binomial test to verify if the proportion of each cell type inside the cell's neighborhood is significantly greater than the global proportion. We observed that the distribution of these putative follicular helper T cells as a percentage of all CD4+ memory T cells (37% to 52%, Fig 5j) is consistent with previous characterizations within the spleen from healthy donors achieved through orthogonal fluorescence-activated cell sorting approaches[26,27].

Discussion

In this paper, we present CRAWDAD, Cell-type Relationship Analysis Workflow Done Across Distances, to quantify cell-type spatial relationships across spatial length scales. We validated CRAWDAD by recapitulating expected cell-type spatial relationships in simulated and real SRO datasets of diverse tissues assayed by diverse SRO technologies. We demonstrated that our tool was able to provide distinct insights compared to existing spatial enrichment and multi-scale analyses. We emphasize that cell-type spatial relationships may vary across spatial scales and such multi-scale characterization enabled by tools like CRAWDAD can reveal distinct insights not apparent in evaluations of spatial relationships that consider only the whole tissue scale. Additionally, we emphasize that such quantified cell-type spatial relationships trends can be used to compare across SRO datasets and demonstrate its application in identifying consistent spatial

trends within mouse brain replicates that are distinct across Bregma locations. We further apply CRAWDAD to characterize cell-type spatial relationships to HuBMAP SRO datasets of the human spleen to identify generally consistent spatial trends reflective of the organization of the red and white pulp but also reproducible patient-specific variation, though the sample sizes evaluated here limit our ability to make general significant conclusions. As atlasing efforts such as HuBMAP[19], the Human Cell Atlas[28], and others continue to profile the spatial organization of cells within tissues, we anticipate identifying significant spatial variation across axes of interest will become more feasible in the future, though additional scalable, comparative meta-analysis tools to integrate statistics from many samples across multiple studies in a manner that is robust to batch effects may be then needed. We expect that the incorporation of quantitative spatial trend metrics such as those provided by CRAWDAD will be useful in such meta-analyses to ultimately facilitate in the identification and characterization of cell-type colocalization relationships in complex tissues to advance our understanding of the relationship between cell-type organization and tissue function.

Although we have demonstrated CRAWDAD to be a potentially useful tool in identifying, characterizing, and comparing cell-type spatial relationships, there are several considerations worth noting as they may influence interpretation. First, CRAWDAD results rely on a few user-defined parameters. In particular, it uses a fixed neighborhood distance d to determine the size of the neighborhood used to consider neighboring cells. In the context of geospatial analysis, such sensitivity of results to the neighborhood distance has been previously characterized as the sensitivity to kernel bandwidth[29]. We note that if the defined d is too small, the neighborhood will only contain cells from the reference cell type. In such a scenario, the total number of neighbor cells would be zero, leading to non-significant results. Alternatively, if d is too large, the neighborhood will encompass all the cells in the sample. In this case, the proportions of cell types

within the neighborhood before and after shuffling will remain the same, leading to non-significant results. Generally, we recommend choosing d based on the biological constraints of the analysis. For example, to identify cell-type spatial relationships that may be relevant to cell-cell interactions, one may choose a neighborhood distance d up to 100 μm to reflect the limits of diffusion of epidermal growth factor that cells may use in paracrine signaling[30]. Additionally, visualizing the neighborhood may be used to guide the choice of d (Supp Fig 8). For example, for mouse cerebellum and embryo SRO datasets analyzed, we highlight how a neighborhood of 10μm would be too small as it does not enclose a significant proportion of the cells given the density of cells in the tissues. On the other hand, a neighborhood of 100μm would be too large as some of the cell types would incorporate all cells of other cell types inside the neighborhood buffer. Hence, a $d =$ 50μm was used for these SRO datasets. In general, the neighborhood distance should be chosen based on guidance from data visualization as well as biological prior knowledge.

Second, to create empirical null backgrounds of cell-type spatial relationships, CRAWDAD shuffles cell-type labels within non-overlapping tiles to create different null backgrounds. Although square tiles are used by default, hexagonal tiles are also available. To evaluate the robustness of trends given these different grid shapes, we created hexagonal tiles in our simulated dataset and repeated analysis (Supp Fig 9a). Comparing the Z-scores obtained at each scale on the different tiles, we noted a high correlation (R = 0.99) across all evaluated scales (Supp Fig 9b), suggesting the shape of the tiles is likely not a key factor in identifying spatial relationships, though both are available as options. The choice of the length scales should reflect the biological analysis of interest. However, choosing values smaller than the neighborhood distance may lead to trivial insignificant results.

Third, since CRAWDAD takes annotated cell-type as input, the quality of the results directly depends on the quality of the annotation. Misannotated cell types could shift the proportions of other cell types inside spatial neighborhoods to alter the spatial relationships identified by CRAWDAD. Thus, cell-type annotations may be evaluated for robustness and cleaned if needed prior to CRAWDAD analysis[31,32]. Or alternatively, identified cell-type spatial relationships may be re-evaluated given multiple potential cell-type annotations to ensure the robustness of identified trends.

Finally, although we have elected to demonstrate CRAWDAD analysis on datasets from select SRO technologies, in general, CRAWDAD is amenable to any SRO technology for which spatial positions and associated labels can be derived. However, we caution that for some multi-cellular spot-based SRO technologies, additional deconvolution or processing may be needed to ensure appropriate interpretation of results. In general, we recommend applying CRAWDAD to datasets with single cell resolution to facilitate interpretation.

Overall, when used appropriately, such cell-type spatial relationship analysis enabled by tools like CRAWDAD will provide another quantitative metric to facilitate the identification, characterization, and comparison of structural differences in tissues across axes of interest such as health and disease or development. Combined with the improvement in cell segmentation, we anticipate that future applications of spatial subsetting analysis such as that achieved with CRAWDAD can enable spatially-informed differential analysis to characterize subtle changes in cell state for cells of the same type colocalized within different microenvironment. Likewise, combined with other tools for identifying spatial niches or domains[33–35], we anticipate such cell-type spatial relationships may be characterized in a niche or domain-specific manner. Ultimately, we anticipate the analysis of SRO data with CRAWDAD can enable a more detailed quantitative

characterization of cell-type spatial organization to contribute to our understanding of how spatial context and tissue architecture vary across health, disease, and development.

Methods

CRAWDAD (Cell-type Relationship Analysis Workflow Done Across Distances) Overview

CRAWDAD characterizes cell-type spatial relationship trends by comparing observed pairwise cell-type spatial relationships to a set of null distributions in which cell-type labels have been shuffled at different length scales.

Creating null distributions at different length scales

To generate empirical null distributions against which observed cell-type spatial relationships can be compared to evaluate for statistical significance, CRAWDAD employs a grid-based cell-type label shuffling strategy. Given a tissue containing cells represented by x-y spatial coordinates with cell-type annotations, we partition the tissue into non-overlapping side-by-side tiles. By default, tiles are squares of area r^2, where r is the size of the spatial length scale of analysis. Then for all cells that reside within the same square, cell-type labels are shuffled to create a null distribution for the given r. These shuffled null distributions are created for multiple rs to achieve a set of empirical null distribution at different length scales. We further create multiple permutations at each length scale by applying different random seeds and a grid-offsetting approach to mitigate

the influence of spatial patterns that would benefit specific grid divisions. Specifically, the offsets are calculated by creating a sequence from 0 to r, in equally spaced intervals of r divided by the number of permutations. In each of the permutations, a different offset of the sequence will be applied. In addition to square tiles, CRAWDAD allows the creation of side-by-side non-overlapping hexagon tiles. In this case, the size of the scale is represented by length of the sides of the hexagon (Supp Fig 9a).

Computing cell-type spatial relationship trends

To evaluate the statistical significance of an observed pairwise cell-type spatial relationship, CRAWDAD uses a binomial testing framework. For a given reference cell-type, CRAWDAD defines neighboring cells as those within a Euclidean distance of a user-defined neighbor distance d (default: 50 units) of any reference cell-type cells. CRAWDAD then calculates the proportion of neighboring cells that are members of a given query cell-type:

$$p_1 = \frac{y_1}{n}$$

where n is the total number of total neighboring cells for a given reference cell-type, and y_1 is the total number of cells of a given query cell-type that are neighboring cells for a given reference cell-type. By default, the reference cells, used to create the neighborhood, are removed from the proportion calculation.

This proportion is also computed for the previously created null distributions:

$$p_2 = \frac{y_2}{n}$$

where y_2 is the total number of cells of the query cell-type that are neighboring cells in the shuffled

null distribution datasets.

A two-sided binomial proportion test is then performed to test the equality of p_1 and p_2

against the alternative that they are not equal:

$H_0: p_1 = p_2$ versus $H_A: p_1 \neq p_2$

This is defined by a test statistic Z, which is:

$$Z = \frac{p_1 - p_2}{\sqrt{\frac{2p(1-p)}{n}}}$$

where:

$$p = \frac{y_1 + y_2}{2n}$$

Defining the significance threshold

We used a significance threshold of 5% (p-value < 0.05 or |Z-score| > 1.96) corrected for multiple testing (Bonferroni method by default) based on the number of unique reference-neighbor cell-type pairs evaluated. In addition, when there were multiple permutations, we considered a Z-score significant if the mean value obtained across permutations is beyond the significance threshold.

Summarizing and visualizing spatial relationship trends

To visually summarize results for all cell-type pairs, CRAWDAD creates a dot plot to show the length scale at which the spatial relationship trend for each cell-type pair first becomes statistically significant, encoded as the size of dots, as well as the associated multiple-testing corrected Z-score, encoded as the color hue of dots. Notably, such summaries do not fully capture the dynamics of pairwise cell-type spatial relationships as a function of length scale. Specifically, if a pairwise cell-type spatial relationship becomes significant at a scale of n, but not significant again at a scale of m (m > n), only the n scale will be represented in the plot. If a relationship is not significant, there will be no dot associated with it.

To visualize the spatial relationship results for a particular cell-type pair across different spatial extents, CRAWDAD uses trend plots where the x-axis represents the length scale and the y-axis represents the Z-score such that the trend represents how the spatial relationship of the cell-type pair changes as the spatial length scales increases. To summarize relationship trends across all evaluated cell-type pairs, CRAWDAD identifies the scale and value of the first Z-score of the trend that is above the significance threshold and plot them as a dot for each reference and neighbor pair and uses a dot plot where the Z-score value is represented by the color hue and the scale is represented by the size of the dot. Smaller scales are represented as larger dots to visually emphasize the potential importance of these small-scale colocalization relationships.

Therefore, to visualize results for a specific pairwise cell-type spatial relationship, CRAWDAD further creates trend plots that show the computed multiple-testing corrected Z-score value as a function of the evaluated length scales. When there are various permutations, the mean multiple-testing corrected Z-score across all permutations and +/- an error bar of one standard deviation is visualized.

Spatial subsetting of cells

CRAWDAD can further assign cells of a given cell-type to subsets based on the enrichment or depletion of cell-types within their neighbors using the same binomial testing framework. Given a tissue containing cells represented as x-y spatial coordinates with cell-type annotations, we again define a neighbor distance d. Given a reference and a query cell type, for every cell of the reference cell-type we perform a one-sided binomial exact test to assess if the proportion of query cell-type among the cell's neighbors are significantly greater than the proportion of the query cell-type in the population. Cells of the given reference cell-type with a p-value below a certain user-defined significance threshold can then be further subtyped as cells of the reference cell-type that are enriched with cells of the query cell type.

Creating, analyzing, and comparing simulated data across methods

Simulating SRO data with manually defined spatial patterns

To simulate a spatially resolved omics dataset, we created 8000 cells randomly positioned from 0 to 2000 microns in the x and y coordinates. We chose four points P = [(250, 250), (250, 750), (750,

250), (750, 750)] to be the centers of the circular neighborhoods defining the cell populations, where d(P) represents the distance from a cell to its closest point in P. We labeled the cells with d(P) <= 100 microns as cell types B or C (50% chance each). Then, we labeled the cells with 100 < d(P) < 300 microns as cell type A. Finally, all the other cells were labeled cell type D. For CRAWDAD, a set of shuffled null distribution were created at length scales of 100 to 1000 separated by 50 microns for 10 permutations. To identify significant trends with multiple testing correction, we used a Z-score threshold of 2.96.

To extend the simulated dataset and incorporate cell-type E, we copied the original cell positions, changed the labels to cell-type E, and placed one copy on the right, one on the top, and one on the top right of the original data. Therefore, the extended dataset has 32000 cells, 24000 from cell type E, and ranges from 0 to 4000 microns in both x and y coordinates. We applied CRAWDAD to this dataset using the same parameters as those from the original simulated dataset analysis but increased the Z-score threshold to 3.09.

Simulating SRO data using Gaussian random fields

To create the simulated datasets with self-enrichment patterns, we followed the procedure previously described[11]. First, we simulate the position of 2000 cells by sampling from a uniform distribution ranging from 0 to 1 for both x and y axis. Then, we randomly split the cells in two groups of 1000 instances each. Using the Matern function with nugget variance of 0.1, shape parameter of 0.5, and smoothness parameter of 0.3, we created a covariance function to generate a Gaussian random field for each group. We binarize each field by assigning positive cells to one cell type and negative cells to the other. Finally, we merge both groups and scaled the cells'

positions to 1000 microns. To generate all the ten datasets, we repeated this process using a different random seed for each.

Comparing methods using simulated data

To benchmark CRAWDAD without relying on a significance threshold we performed a relative comparison between the relationship trends. We classified a cell-type as enriched in the neighborhood of the reference cell type if it had the trend with the highest area under the curve (AUC) value in the reference cell-type trend plot. Likewise, we classified a cell type as depleted if it had the most negative AUC value. We focused on measuring each method's capacity to distinguish trends, not the ability to identify statistically significant results.

Analyzing real SRO data

Analysis of the mouse cerebellum

A pre-processed subset of a Slide-seqV2 dataset collected from a ~3000μm-by-~2500μm section of the mouse cerebellum was obtained from the original[5]. This dataset contained 10,098 beads with x-y coordinates and 19 cell-type annotations previously predicted by RCTD[14]. Poorly represented cell types defined as those being annotated in less than 20 beads (Choroid, Candelabrum, Ependymal, Globular, Macrophages) were not considered in the CRAWDAD cell type colocalization, resulting in 14 remaining cell types.

For CRAWDAD, a set of shuffled null distributions were created at length scales of 100, 200, 300, 400, 500, 600, 700, 800, 900, 1000 microns for 10 permutations. A neighbor distance of 50 microns was used to evaluate every pairwise combination of cell-types at each length scale. To identify significant trends with multiple testing correction, we used a Z-score threshold of 3.81.

Analysis of the developing mouse embryo

A pre-processed subset of the seqFISH data of an 8-12 somite stage embryo[4] (Embryo 1) was obtained from the original publication. This ~1000μm-by-1600μm dataset contained 19416 cells with x-y coordinates and 22 cell-type annotations. Coordinates provided in nanometers were converted to microns by multiplying by 1000.

For CRAWDAD, a set of shuffled null distributions were created at length scales of 100 to 1000 by 50 microns for 10 permutations. A neighbor distance of 50 microns was used to evaluate every pairwise combination of cell-types at each length scale. To identify significant trends with multiple testing correction, we used a Z-score threshold of 3.88.

Analysis of the human breast cancer

We collected the 7520.95μm-by-5471.17μm Xenium breast cancer dataset (in situ sample 1, replicate 1) and with annotated cell types from the original publication[6]. Supervised cell type annotations were used. We filtered the original data by removing cells with less than 3 gene counts, obtaining 162107 cells with x-y coordinates and 20 cell-type annotations.

For CRAWDAD, a set of shuffled null distributions were created at length scales of 100 to a 1000 by intervals of 100 microns for 3 permutations. A neighbor distance of 50 microns was used to evaluate every pairwise combination of cell-types at each length scale. To identify significant trends with multiple testing correction, we used a Z-score threshold of 3.84.

Analysis of the mouse brains

We obtained the nine MERFISH mouse brain datasets from the Vizgen Data Release V1.0. May 2021[7] with cell types previously annotated through unified clustering[18]. We filtered the original data by removing cells with less than 3 gene counts and merging sub-cell types. The resulting number of cells and cell-type annotations by sample is provided below:

Location	Replicate	Number of Cells	Number of Cell Types	Tissue Size
1	1	78329	13	9036.87x 6326.88
	2	88884	13	8060.09x 9936.43
	3	84635	14	8504.56x 8249.1
2	1	83546	14	8883.69x 7113.93
	2	84171	14	8867.34x 9316.67
	3	85957	14	9147.76x 6980.63
3	1	70844	14	7058.34x 7829.3
	2	83461	14	8952.54x 6747.24
	3	74866	14	8952.54x 6747.24

For CRAWDAD, a set of shuffled null distributions were created at length scales of 100 to a 1000 by intervals of 100 microns for 3 permutations. A neighbor distance of 50 microns was used to evaluate every pairwise combination of cell-types at each length scale.

Analysis of the human spleen

Pre-processed and compensated Akoya CODEX datasets of 6 human spleens tissue sections ranging from 3550.24μm-by-3423.43μm to 4564.7μm-by-3423.43μm in size from 3 different

donors were downloaded from the HuBMAP Data Portal (https://portal.hubmapconsortium.org/) corresponding to dataset IDs: HBM389.PKHL.936, HBM772.XXCD.697, HBM556.KSFB.592, HBM825.PBVN.284, HBM568.NGPL.345, and HBM342.FSLD.938. These datasets contained protein expression for 28 markers, x-y coordinates, and cell segmentation area measurements for 154,446, 150,311, 152,896, 130,584, 177,777, and 226,384 segmented cells, respectively. Protein expression was normalized by cell area and $\log_{10}$ transformed with a pseudocount of 1.

Unified clustering and cell-type annotation

Using dataset HBM389.PKHL.936, cells were clustered via Louvain graph-based clustering[36] based on a nearest neighbor-graph with k = 50. Protein expression values were summed together for cells assigned to each cluster, and then the values were scaled across protein expression measurements within each cluster. The scaled expression values were used to assign cell-type annotations, which initially resulted in 13 cell types and one unlabeled group. Outer and inner Follicular B cells annotations were combined into a single Follicular B cells annotation. Linear discriminant analysis (LDA) was performed to transfer cell-type labels between the datasets. Prior to label transfer, paired donor datasets HBM556.KSFB.592 and HBM568.NGPL.345, and HBM825.PBVN.284 and HBM342.FSLD.938 were harmonized[37] due to observed batch effects. LDA cell-type label transfers were done between the following reference and query datasets: HBM389.PKHL.936 -> HBM772.XXCD.697, HBM389.PKHL.936 -> HBM556.KSFB.592, HBM389.PKHL.936 -> HBM825.PBVN.284, HBM556.KSFB.592 -> HBM568.NGPL.345, HBM825.PBVN.284 -> HBM342.FSLD.938.

CRAWDAD analysis of the human spleen

For CRAWDAD, a set of shuffled null distributions were created at resolutions of length scales of 100 to a 1750 by intervals of 50 microns for 10 permutations. A neighbor distance of 50 microns was used to evaluate every pairwise combination of cell-types at each scale. The corrected Z-score threshold used was 3.58.

Spatial subsetting of the human spleen

CD4+ memory T cells were further subsetted based on their proximity to Follicle B cells using a one-sided exact binomial test, a neighbor distance defined as 50 microns and a p-value threshold of 0.05. With the subsets, we calculated the proportion of CD4+ memory T cells near Follicle B cells with respect to all CD4+ memory T cells and compared across datasets.

Comparing across different samples

To compare different samples, we opted to use the area under the curve (AUC) of the Z-score trend to represent each relationship instead of the scale of when the relationship reaches significance as not all of them do. We represented each sample by the AUC values of each cell-type pair, creating an AUC high-dimensional space. By applying principal component analysis to this space, we used the first two components to visualize the samples. In this case, instances that are similar in the high-dimensional space should also be similar in the low-dimensional one. Additionally, we investigated the variance of AUC across samples by plotting the variance for each cell-type pair in a dot plot. Lastly, we visualized the relationship trends for the cell-type pair with highest AUC variance across conditions.

Analysis with other methods

Ripley's Cross-K Analysis

Ripley's Cross K function draws a circular neighborhood around each reference cell, counts the number of cells of each type inside this region, and divide it by the cell-type density. This value is compared to the theoretical K. The multi-scale aspect of this analysis comes from varying the neighborhood size. Additionally, cells in the border of the tissue will consider areas that do not present any cell, requiring the application of border correction methods to mitigate this effect. We used the spatstat (version 3.0-6) package[38] to compute different Ripley's Cross-K values for each pairwise combination of cell types. To compare with the theoretical K and perform border correction, we subtracted the theoretical K for a Poisson homogeneous processes from the isotropic edge corrected Ripley's Cross-K. For consistency in visualization, we set the maximum radius size to be the same as the maximum length scale evaluated in CRAWDAD.

Squidpy's Neighborhood Enrichment

We used Squidpy[10] (version 1.2.3) to apply its neighborhood enrichment implementation of the approach described by Schapiro *et al.*[9] We defined the spatial neighbors using a radius of 50 and calculated Squidpy's neighborhood enrichment using default parameters. The results were plotted as a heatmap of Z-scores.

Squidpy's Cooccurrence Probability

Squidpy[10] implements the co-occurrence probability method originally presented in Tosti *et al.*[13] The function works by drawing annular neighborhoods around each cell of the reference cell type. Then, it calculates the probability of a cell type being enriched in that region. The multi-scale aspect of this analysis comes from varying the neighborhood size.

Using Squidpy (version 1.2.3) and its co_occurrence function, we calculated the co-occurrence probability of clusters for each cell type. For consistency in visualization, we set the maximum distance to be the same as the maximum length scale evaluated in CRAWDAD.

Code availability

CRAWDAD is available as an open-source R package at https://github.com/jefworks-lab/crawdad with additional documentation and tutorials available at https://jef.works/CRAWDAD/. Code to reproduce the analyses and results of this study is available on GitHub at https://github.com/rafaeldossantospeixoto/crawdad_revision_analysis.

Conflicts of interest

None declared.

References

1. Mitra, P. P. The Circuit Architecture of Whole Brains at the Mesoscopic Scale. *Neuron* **83**, 1273–1283 (2014).

2. Elhanani, O., Ben-Uri, R. & Keren, L. Spatial profiling technologies illuminate the tumor microenvironment. *Cancer Cell* **41**, 404–420 (2023).

3. Manz, B. N. & Groves, J. T. Spatial organization and signal transduction at intercellular junctions. *Nat Rev Mol Cell Biol* **11**, 342–352 (2010).

4. Lohoff, T. *et al.* Integration of spatial and single-cell transcriptomic data elucidates mouse organogenesis. *Nat Biotechnol* **40**, 74–85 (2022).

5. Stickels, R. R. *et al.* Highly sensitive spatial transcriptomics at near-cellular resolution with Slide-seqV2. *Nat Biotechnol* **39**, 313–319 (2021).

6. Janesick, A. *et al.* High resolution mapping of the tumor microenvironment using integrated single-cell, spatial and in situ analysis. *Nat Commun* **14**, 8353 (2023).

7. MERFISH Mouse Brain Receptor Map. *Vizgen Data Release V1.0. May 2021* https://info.vizgen.com/mouse-brain-map.

8. Goltsev, Y. *et al.* Deep Profiling of Mouse Splenic Architecture with CODEX Multiplexed Imaging. *Cell* **174**, 968-981.e15 (2018).

9. Schapiro, D. *et al.* histoCAT: analysis of cell phenotypes and interactions in multiplex image cytometry data. *Nat Methods* **14**, 873–876 (2017).

10. Palla, G. *et al.* Squidpy: a scalable framework for spatial omics analysis. *Nat Methods* **19**, 171–178 (2022).

11. Viladomat, J., Mazumder, R., McInturff, A., McCauley, D. J. & Hastie, T. Assessing the significance of global and local correlations under spatial autocorrelation: A nonparametric approach. *Biometrics* **70**, 409–418 (2014).

12. Ripley, B. D. The second-order analysis of stationary point processes. *J Appl Probab* **13**, 255–266 (1976).

13. Tosti, L. *et al.* Single-Nucleus and In Situ RNA–Sequencing Reveal Cell Topographies in the Human Pancreas. *Gastroenterology* **160**, 1330-1344.e11 (2021).

14. Cable, D. M. *et al.* Robust decomposition of cell type mixtures in spatial transcriptomics. *Nat Biotechnol* **40**, 517–526 (2022).

15. Alberts, B. *et al.* Looking at the Structure of Cells in the Microscope. in *Molecular Biology of the Cell* (Garland Science, New York, 2002).

16. Bellamy, T. C. Interactions between Purkinje neurones and Bergmann glia. *The Cerebellum* **5**, 116–126 (2006).

17. Wang, P. *et al.* The spatial distribution of immune cell subpopulations in hepatocellular carcinoma. *Cancer Sci* **113**, 423–431 (2022).

18. Clifton, K. *et al.* STalign: Alignment of spatial transcriptomics data using diffeomorphic metric mapping. *Nat Commun* **14**, 8123 (2023).

19. Jain, S. *et al.* Advances and prospects for the Human BioMolecular Atlas Program (HuBMAP). *Nat Cell Biol* (2023) doi:10.1038/s41556-023-01194-w.

20. Lewis, S. M., Williams, A. & Eisenbarth, S. C. Structure-function of the immune system in the spleen. *Sci Immunol* **4**, (2019).

21. Nolte, M. A., 't Hoen, E. N. M., Van Stijn, A., Kraal, G. & Mebius, R. E. Isolation of the intact white pulp. Quantitative and qualitative analysis of the cellular composition of the splenic compartments. doi:10.1002/1521-4141.

22. Cheng, H.-W. *et al.* Origin and differentiation trajectories of fibroblastic reticular cells in the splenic white pulp. *Nat Commun* **10**, 1739 (2019).

23. Currlin, S. *et al.* Immune, endothelial and neuronal network map in human lymph node and spleen. *bioRxiv* 2021.10.20.465151 (2022) doi:10.1101/2021.10.20.465151.

24. Korsunsky, I. *et al.* Fast, sensitive and accurate integration of single-cell data with Harmony. *Nat Methods* **16**, 1289–1296 (2019).

25. Garside, P. *et al.* Visualization of Specific B and T Lymphocyte Interactions in the Lymph Node. *Science (1979)* **281**, 96–99 (1998).

26. Vecchione, A. *et al.* Reduced Follicular Regulatory T Cells in Spleen and Pancreatic Lymph Nodes of Patients With Type 1 Diabetes. *Diabetes* **70**, 2892–2902 (2021).

27. Zhao, J. *et al.* Hyperactive Follicular Helper T Cells Contribute to Dysregulated Humoral Immunity in Patients With Liver Cirrhosis. *Front Immunol* **10**, (2019).

28. Regev, A. *et al.* The Human Cell Atlas. *Elife* **6**, (2017).

29. O'Sullivan, D. & Unwin, D. J. *Geographic Information Analysis*. (Wiley, 2010). doi:10.1002/9780470549094.

30. Handly, L. N., Pilko, A. & Wollman, R. Paracrine communication maximizes cellular response fidelity in wound signaling. *Elife* **4**, (2015).

31. Charrad, M., Ghazzali, N., Boiteau, V. & Niknafs, A. NbClust: An R Package for Determining the Relevant Number of Clusters in a Data Set. *J Stat Softw* **61**, (2014).

32. Taskesen, E. clusteval is a python package for unsupervised cluster validation. Preprint at https://erdogant.github.io/clusteval (2020).

33. Hickey, J. W. *et al.* Organization of the human intestine at single-cell resolution. *Nature* **619**, 572–584 (2023).

34. Dong, K. & Zhang, S. Deciphering spatial domains from spatially resolved transcriptomics with an adaptive graph attention auto-encoder. *Nat Commun* **13**, 1739 (2022).

35. Hu, J. *et al.* SpaGCN: Integrating gene expression, spatial location and histology to identify spatial domains and spatially variable genes by graph convolutional network. *Nat Methods* **18**, 1342–1351 (2021).

36. Blondel, V. D., Guillaume, J.-L., Lambiotte, R. & Lefebvre, E. Fast unfolding of communities in large networks. (2008) doi:10.1088/1742-5468/2008/10/P10008.

37. Korsunsky, I. *et al.* Fast, sensitive and accurate integration of single-cell data with Harmony. *Nat Methods* **16**, 1289–1296 (2019).

38. Baddeley, A., Rubak, E. & Turner, R. *Spatial Point Patterns: Methodology and Applications with R*. (Chapman and Hall/CRC Press, 2015).

Figures
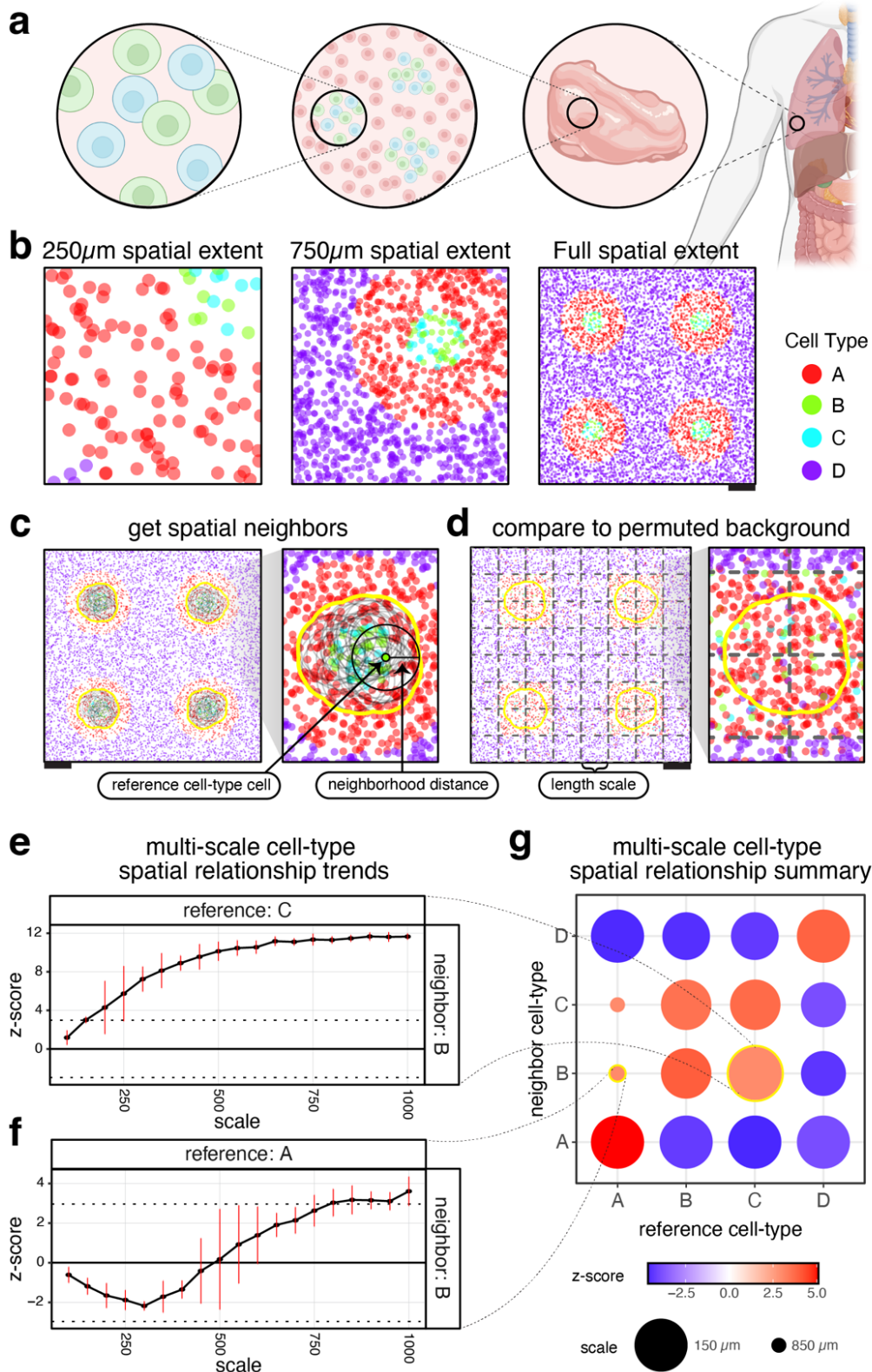
Figure 1. Motivating Cell-type Relationship Analysis Workflow Done Across Distances (CRAWDAD) using simulated data. **a.** Illustration of the cell-type spatial relationships found at different length scales. **b.** Simulated spatial omics tissue data, visualized at different scales. Each point is a cell, colored by cell type. Scale bars correspond to 250μm. **c.** Representation of the creation of the neighborhood and the null background. CRAWDAD draws a circle (neighborhood distance as the radius) around each cell of the reference cell type and merges them into one neighborhood. **d.** CRAWDAD creates a grid of side-by-side tiles (length scale defined as the side length for square pixels and the distance between opposite edges for hexagonal pixels) and shuffles the labels inside each tile to create the null background. **e.** The multi-scale spatial relationship trend plot for reference cell-type C and neighbor cell-type B. The horizontal dotted lines represent the z-score significance threshold corrected for multiple testing (Z-score = ±2.96). The red bars denote the standard error for the z-score estimated using permutations. **f.** The multi-scale spatial relationship trend plot for reference cell-type A and neighbor cell-type B. **g.** Summary visualization all cell-type spatial relationships. The size of the dot represents the scale in which a neighbor cell-type first reaches a significant spatial relationship with respect to a reference cell-type. The color of the dot is the z-score at such scale.

Figure 2. CRAWDAD characterizes cell-type spatial relationships in the mouse cerebellum assayed by Slide-seqV2 and the mouse embryo assayed by seq-FISH. **a**. Spatial visualization of cell type annotations from RCTD in the cerebellum. Scale bars correspond to 250μm. **b**. Summary visualization all cell-type spatial relationships in the cerebellum data. Select cell types highlighted to correspond with (c-e). **c-e**. The multi-scale spatial relationship trend plot for Purkinje neurons as the reference cell type for (**c**) CRAWDAD, (**d**) Ripley's K Cross and (**e**) Squidpy co-occurrence implementation of Tosti et al. with neighboring cell-types Bergmann glia and Oligodendrocytes highlighted in red and blue respectively. All other neighboring cell-types in grey. **f**. Spatial visualization of annotated cell types in the embryo data. Scale bars correspond to 250μm. **g**. Summary visualization all cell-type spatial relationships in the embryo data. Select cell types highlighted to correspond with (h-j). **h-j**. The multi-scale cell-type spatial relationship trend plot for Endothelium cells as the reference cell type for (**h**) CRAWDAD, (**i**) Ripley's K Cross and (**j**) Squidpy co-occurrence implementation of Tosti et al. with neighboring cell-types Cardiomyocytes and Lateral plate mesoderm highlighted in red and blue respectively. All other neighboring cell-types in grey.
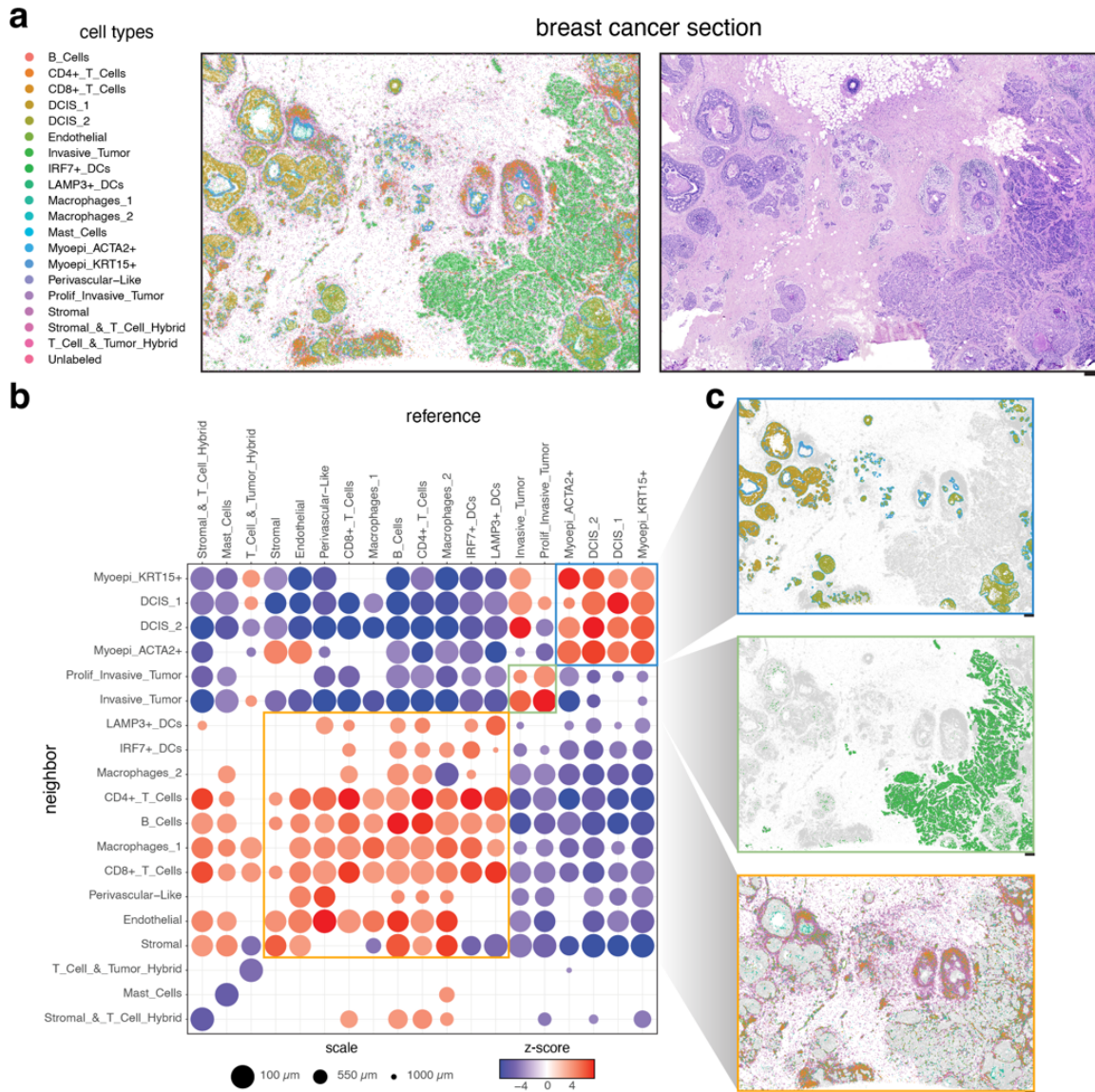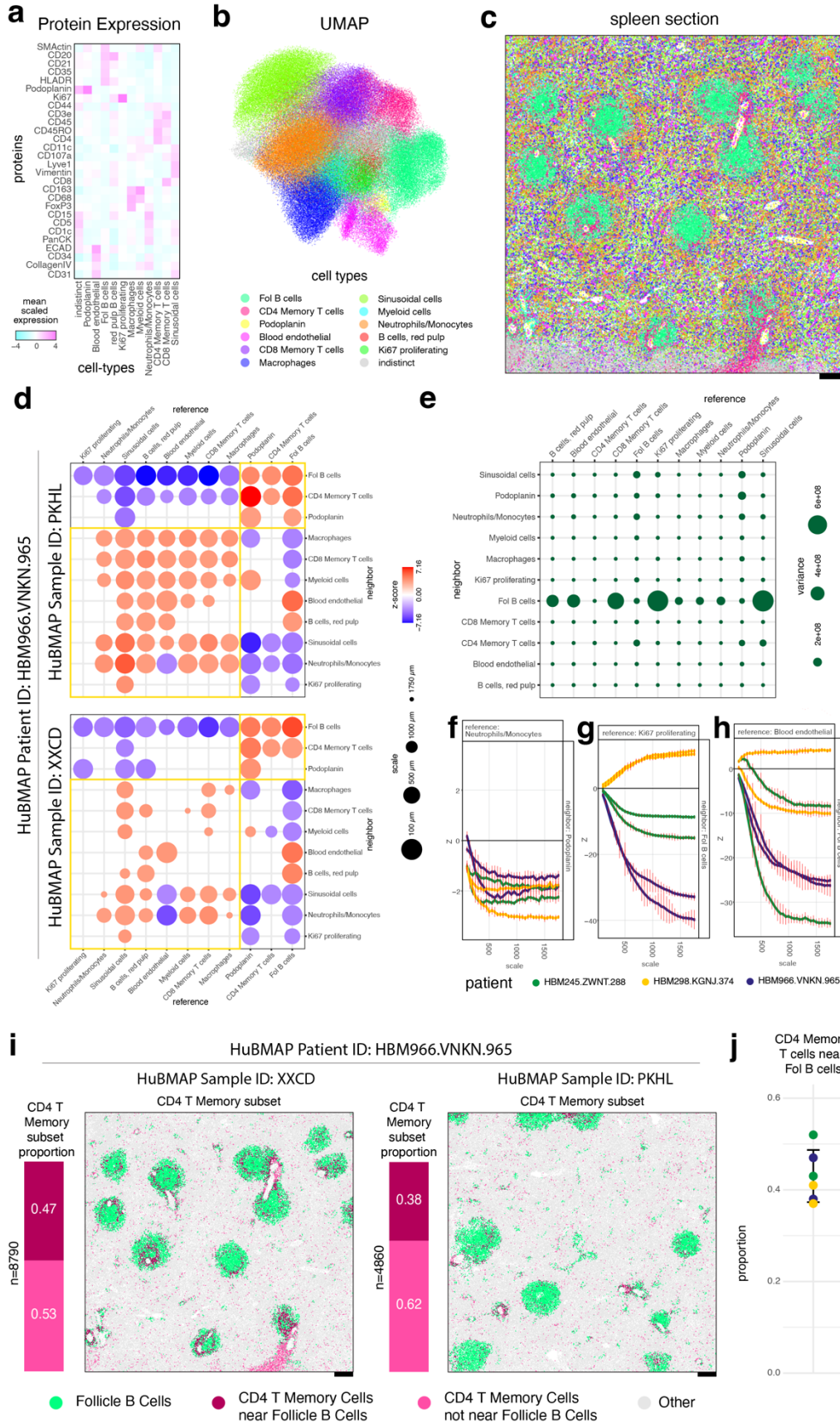
Fig 3. CRAWDAD characterizes cell type spatial relationships in breast cancer assayed by Xenium. **a**. Spatial visualization of annotated cell types (left) with corresponding histology image (right). **b**. Summary visualization all cell-type spatial relationships in the breast cancer data. Select groups of consistently colocalized cell-types is outlined by a unique color. **c**. Spatial visualization of the consistently colocalized cell-types. Plots for each tissue structure are outlined by the corresponding color in (b). Scale bars correspond to 250μm.
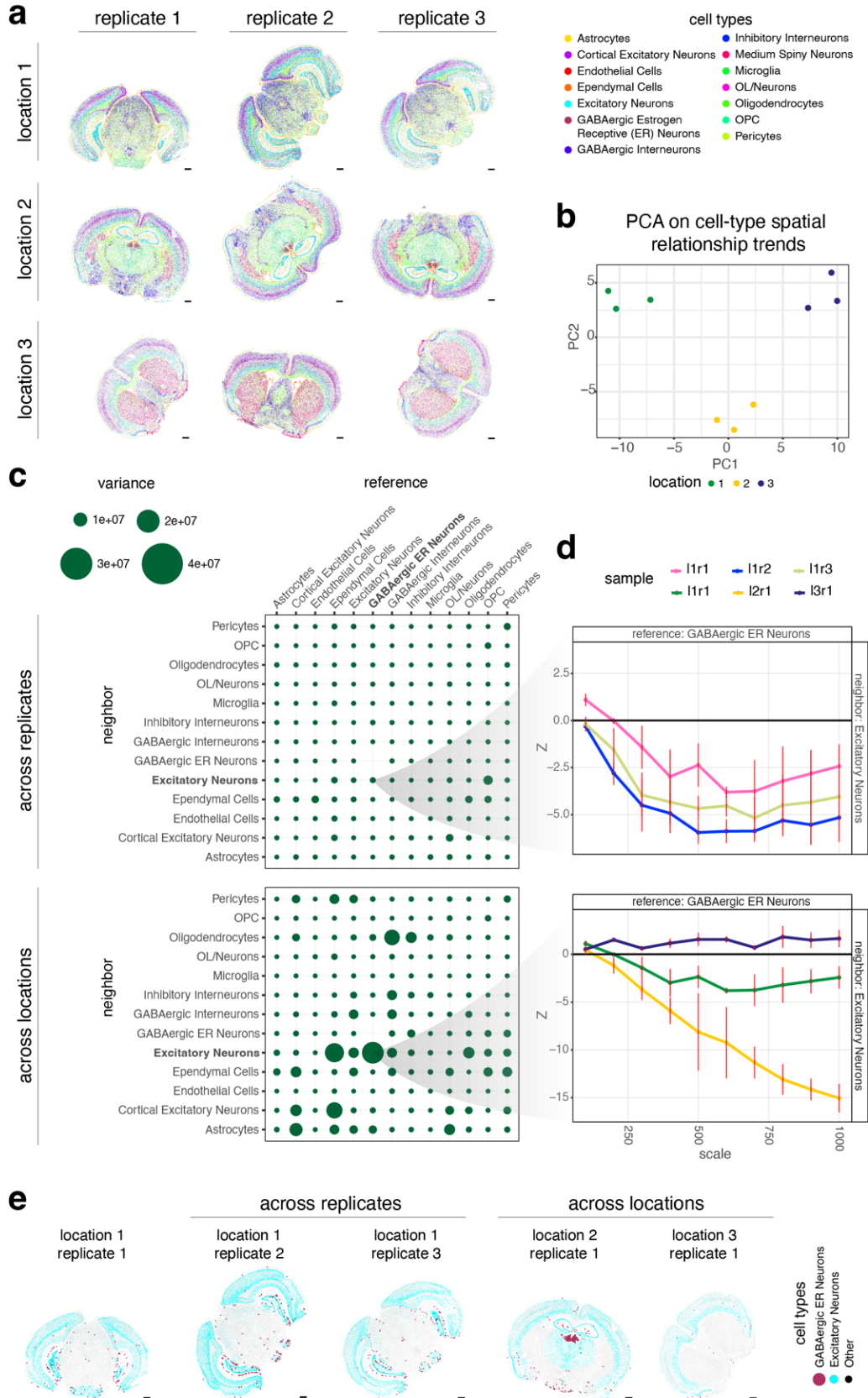
Figure 4. CRAWDAD enables comparison of spatial relationships across different tissue sections of the mouse brain assayed by MERFISH. **a**. Spatial visualization of annotated cell types in each sample. Scale bars correspond to 1000μm. **b**. Visualization of each sample in the principal component space with the first two principal components calculated using the standardized AUC of each multi-scale cell-type spatial relationship trend. **c**. Variability of multi-scale cell-type spatial relationship trends calculated as the variance of the AUC values across replicates (top) and locations (bottom). **d**. The multi-scale cell-type spatial relationship trend plot of GABAergic Estrogen-Receptive (ER) Neurons as reference and Excitatory Neurons as neighbor for samples of replicates from the same location (top) and different locations (bottom). **e**. Spatial visualization of the GABAergic ER Neurons and Excitatory Neurons in replicates from the same location (left) and different locations (right).

Figure 5. CRAWDAD characterize cell-type spatial relationships in the human spleen assayed by CODEX. **a.** Heatmap of marker protein expression for annotated cell types. **b.** UMAP reduced-dimensional visualization of annotated cell-types. **c.** Spatial visualization of annotated cell-types in one representative tissue section. Scale bars correspond to 250μm. **d.** Summary visualization of the multi-scale cell-type spatial relationship analysis for tissue sections PKHL and XXCD from patient HBM966.VNKN.965. Cell types consistently colocalized in the white and red bulk are highlighted with small and large squares respectively. **e**. Variability of multi-scale cell-type spatial relationship trends calculated as the variance of the AUC values across samples. The multi-scale cell-type spatial relationship trend plots are shown for select cell-type pairs exhibiting **f.** low variability across different samples, **g.** high variability across patients but low variability within replicates, and **h.** high variability across samples including within patients. **i.** Subset of CD4+ Memory T cells near Follicle B cells. The number of CD4+ Memory T cells (n) and the proportion of subsets (left) and spatial visualization of subsets (right) in tissue sections PKHL and XXCD from patient HBM966.VNKN.965. **j.** Proportion of CD4+ Memory T cells near Follicle B cells over all CD4+ Memory T cells in each sample.
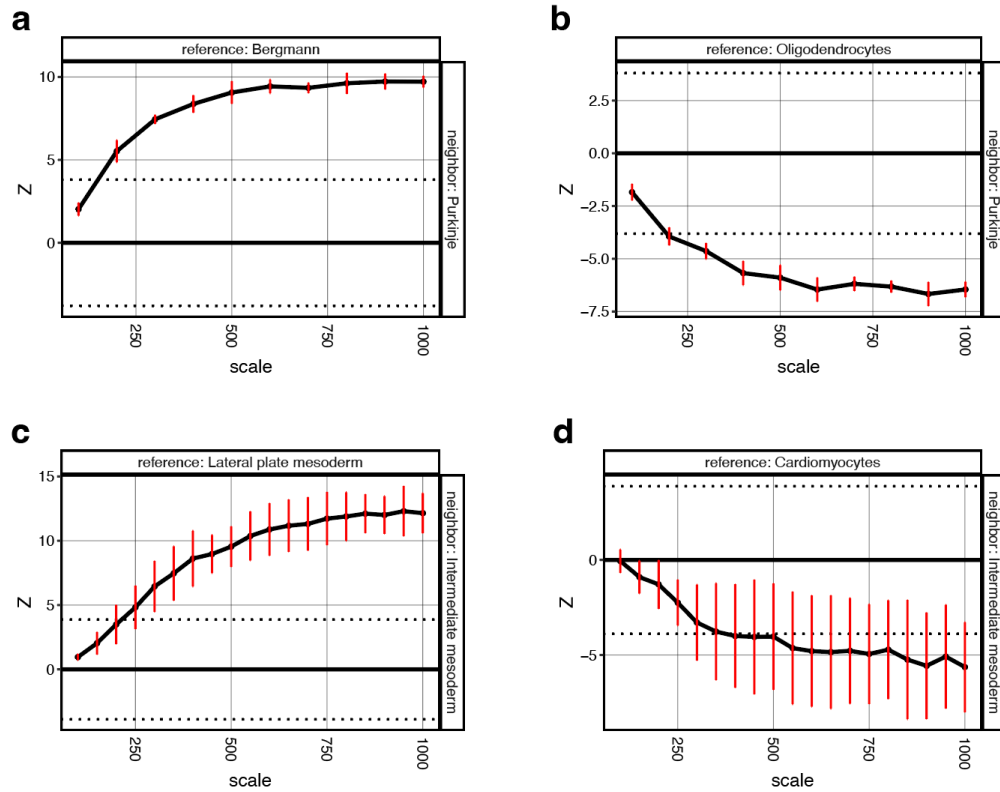
Supplementary Figures
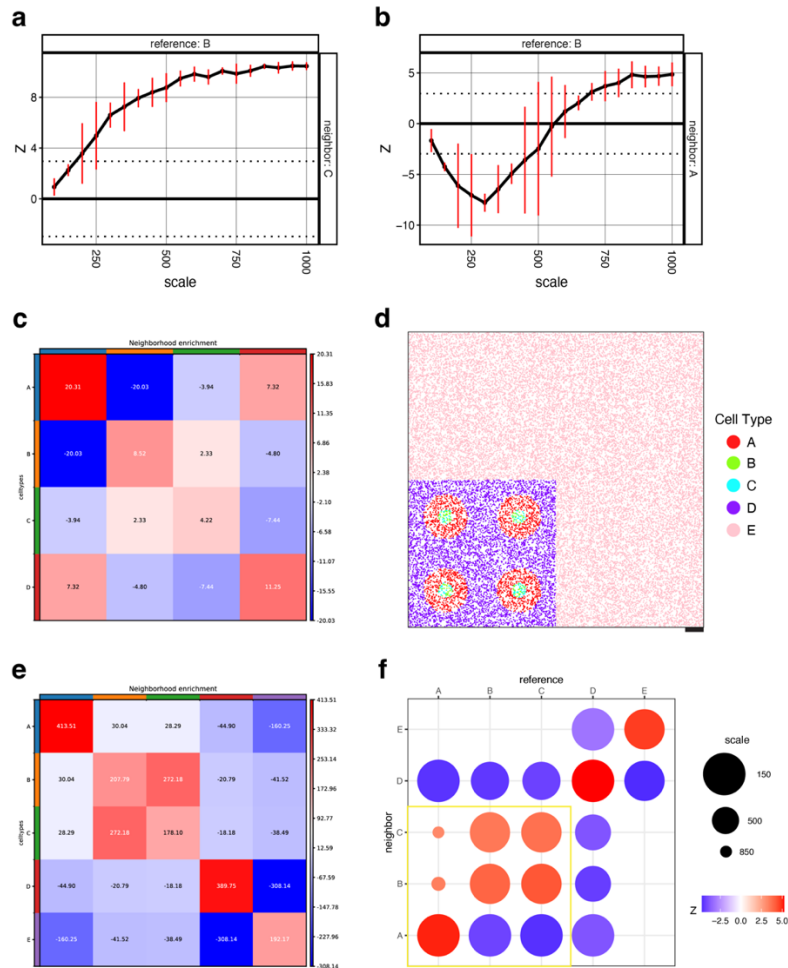
Supplementary Figure 1. CRAWDAD and Squidpy's neighborhood enrichment implementation on simulated data. CRAWDAD's multi-scale spatial relationship trend plot for **a.** reference cell-type B and neighbor cell-type C and **b.** for reference cell-type B and neighbor cell-type A. **c.** Squidpy's neighborhood enrichment analysis on the simulated data. **d.** New simulated data that included cell-type E contouring the previous original dataset. **e.** Squidpy's neighborhood enrichment analysis on the new simulated data in (d) shows changing cell-type relationships compared to (c). **f.** Summary visualization of CRAWDAD's multi-scale cell-type spatial relationship analysis of the new simulated data. The yellow box highlights that the cell-type relationships found in the analysis of the original simulated data were maintained.
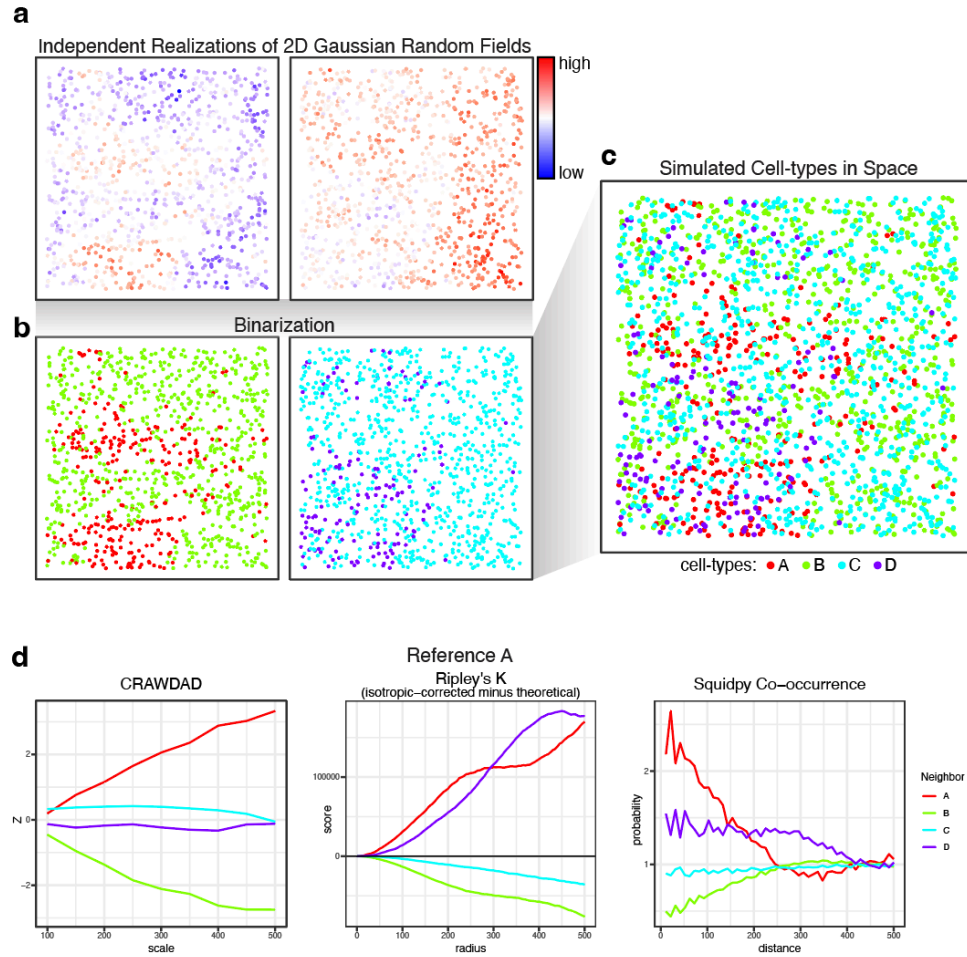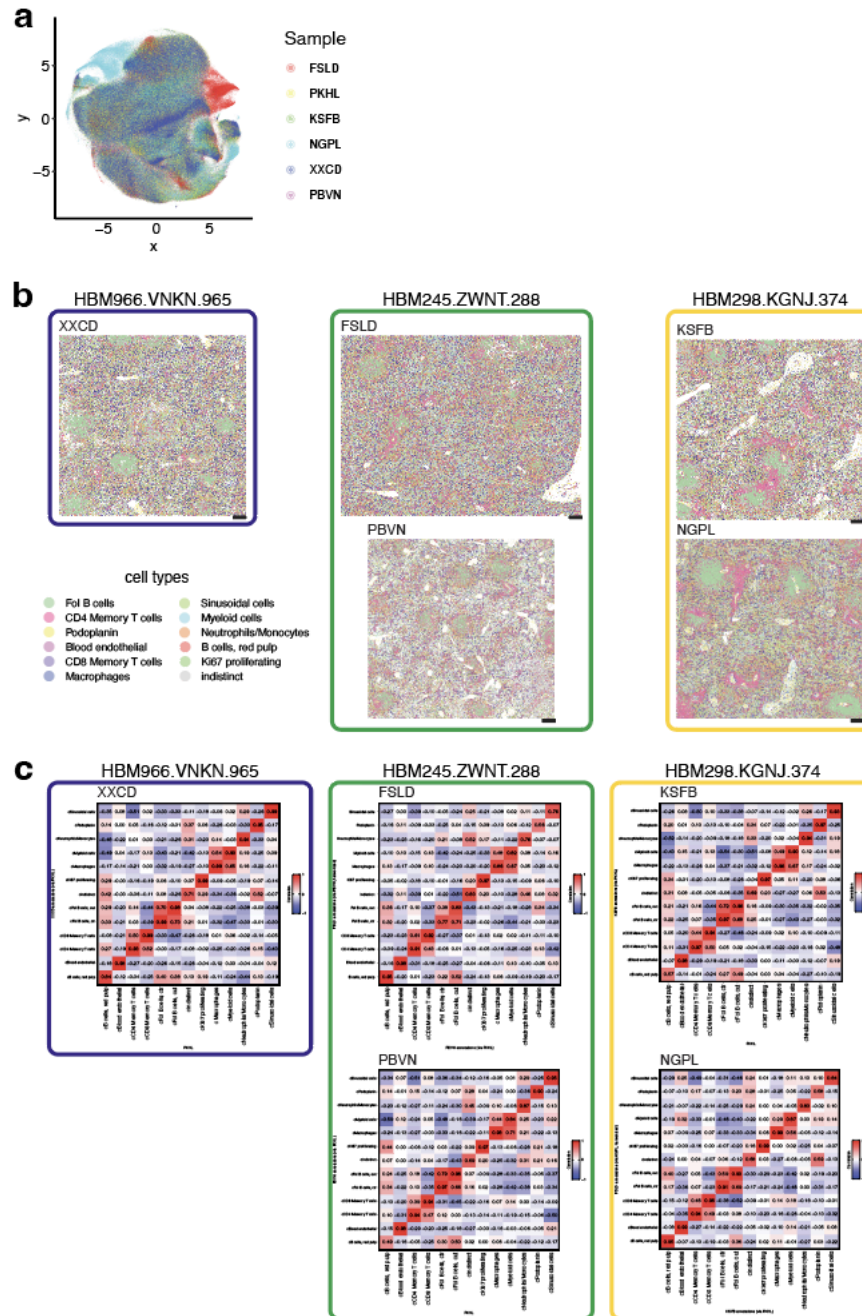
Supplementary Figure 2. Creation of the simulated dataset. **a**. Two independent Gaussian random fields with uniformly sampled spatial positions representing 1000 cells. **b**. These spatial positions are assigned a cell type based on the random field's value. **c**. Both fields are combined to generate one dataset with 4 cell-types. **d**. Relationships trends obtained by each method using cell-type A as the reference cell-type.
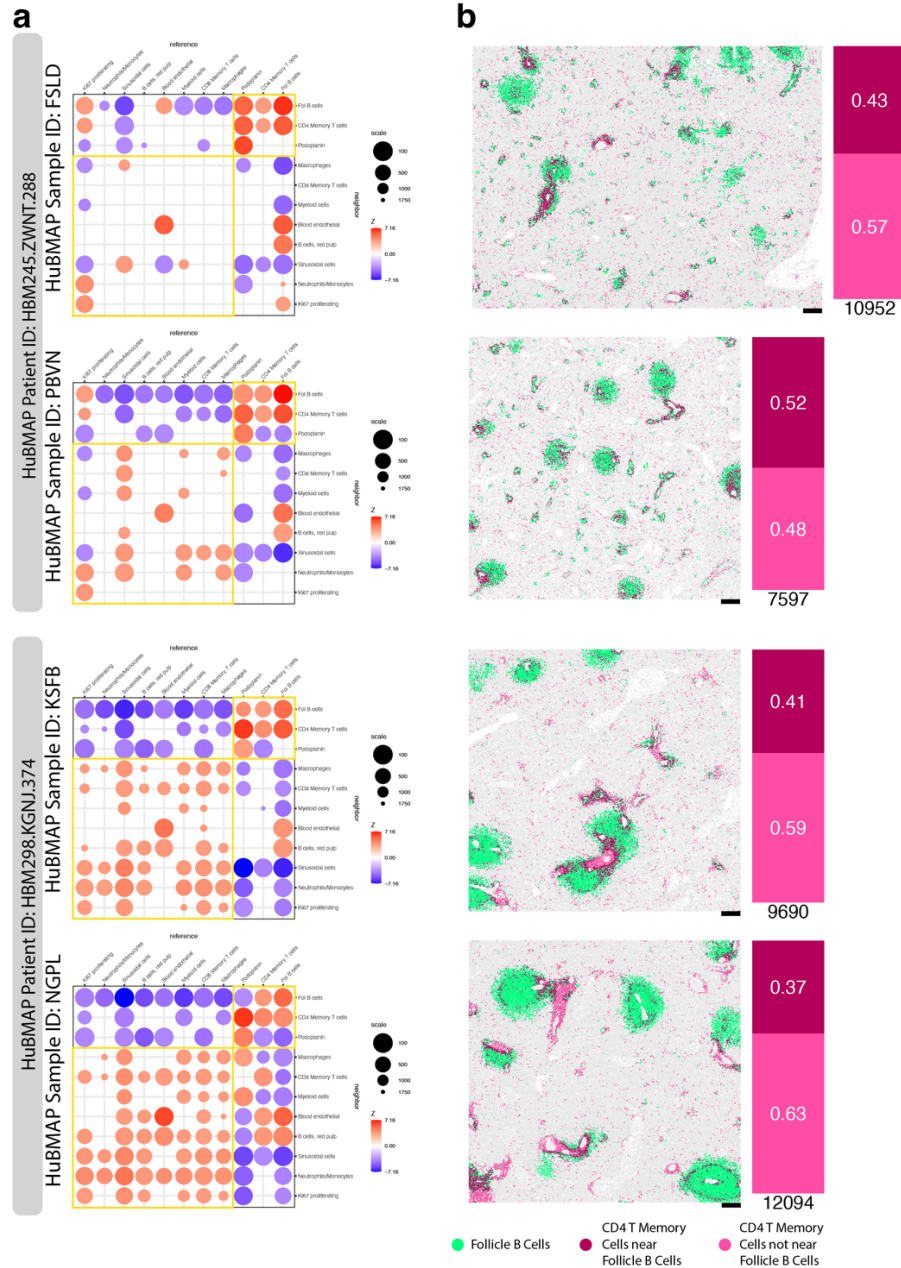
Supplementary Figure 3. Complementary CRAWDAD analysis of the mouse cerebellum and mouse embryo datasets. **a-d**. The multi-scale spatial relationship trend plot for (**a**) reference cell-type Bergmann glia and neighbor cell-type Purkinje neurons; (**b**) reference cell-type Oligodendrocytes and neighbor cell-type Purkinje neurons; (**c**) reference cell-type lateral plate mesoderm and neighbor cell-type intermediate plate mesoderm; (**d**) reference cell-type cardiomyocyte and neighbor cell-type intermediate plate mesoderm.
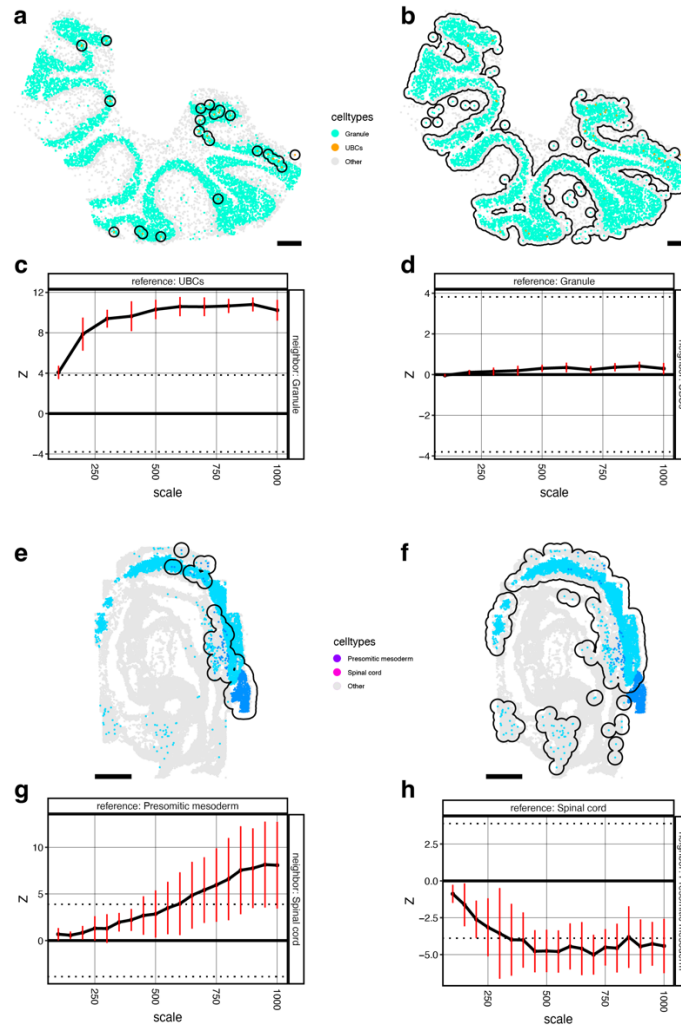
Supplementary Figure 4. Sample asymmetric cell-type spatial relationships. Spatial visualization of cells in the cerebellum with the neighborhood of UBCs (**a**) and Granule cells (**b**) outlined. CRAWDAD's multi-scale spatial relationship trend plot for UBCs and Granule cells with UBCs as the reference cell-type and Granule cells as the neighboring cell-type (**c**) and vice versa (**d**). Spatial visualization of cells in the embryo with the neighborhood of presomitic mesoderm cells (**e**) and spinal cord cells (**f**) outlined. CRAWDAD's multi-scale spatial relationship trend plot for presomitic mesoderm cells and spinal cord cells with presomitic mesoderm cells as the reference cell-type and spinal cord cells as the neighboring cell-type (**g**) and vice versa (**h**). Scale bars correspond to 250μm.
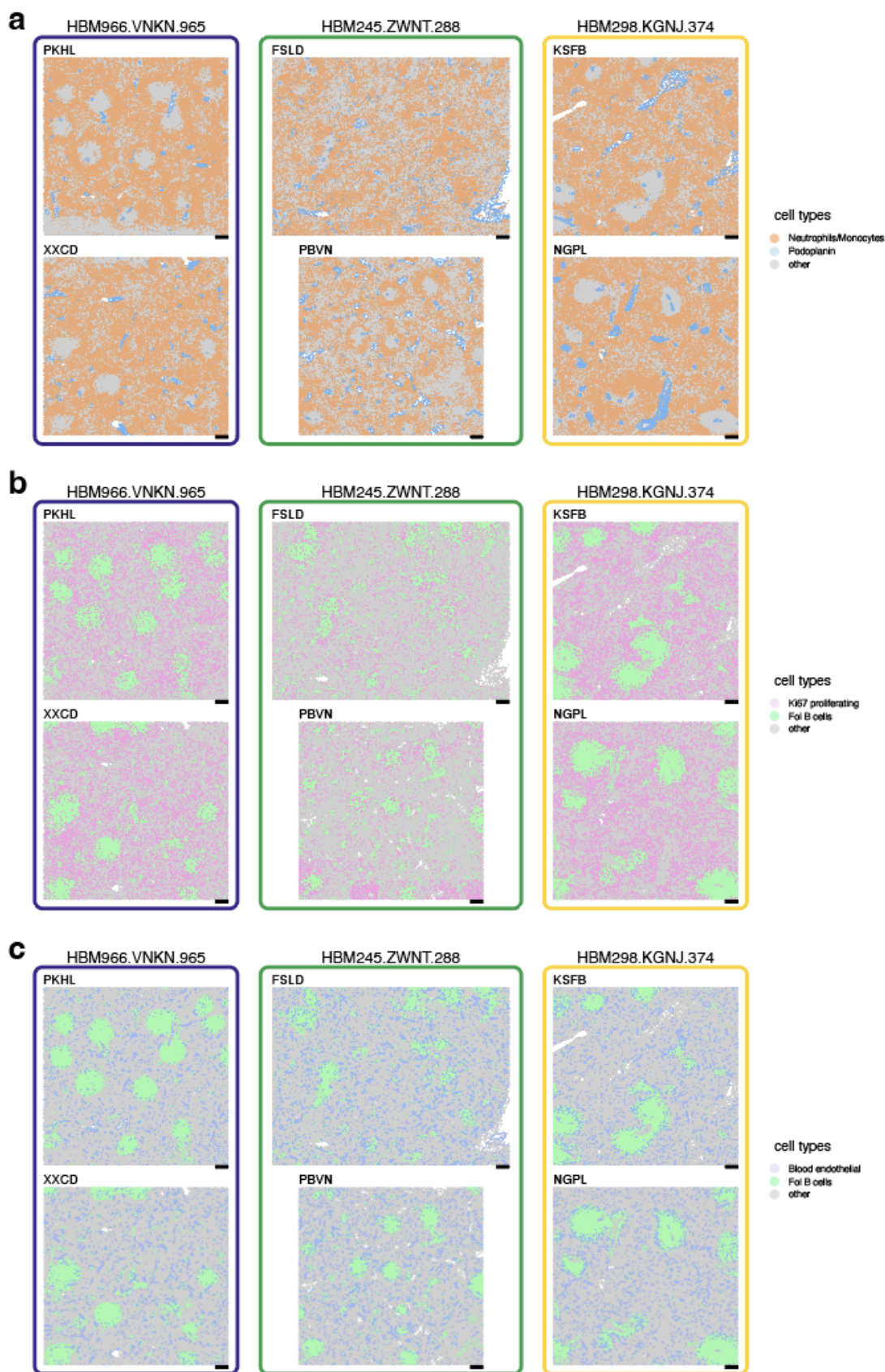
Supplementary Figure 5. CODEX Human Spleen Samples. **a.** Reduced-dimension visualization of the samples. **b.** Spatial visualization of cell types in the different samples and patients. **c.** Heatmaps visualizing transcriptional correlations between label-transferred cell-types in spleen samples and the originally annotated cell-types in reference spleen sample PKHL. Scale bars correspond to 250μm.

Supplementary Figure 6. Analysis of other spleen samples. **a.** Summary visualization of the multi-scale cell-type spatial relationship analysis for datasets FSLD and PBVN from patient HBM245.ZWNT.288 and for datasets KSFB and NGPL from patient HBM298.KGNJ.374. **b.** On the left, the spatial visualization of the subsets of CD4+ Memory T cells near and not near Follicle B cells and Follicle B cells. On the right, the number of CD4+ Memory T cells (n) and the proportion of those that are near Follicle B cells. Scale bars correspond to 250μm.
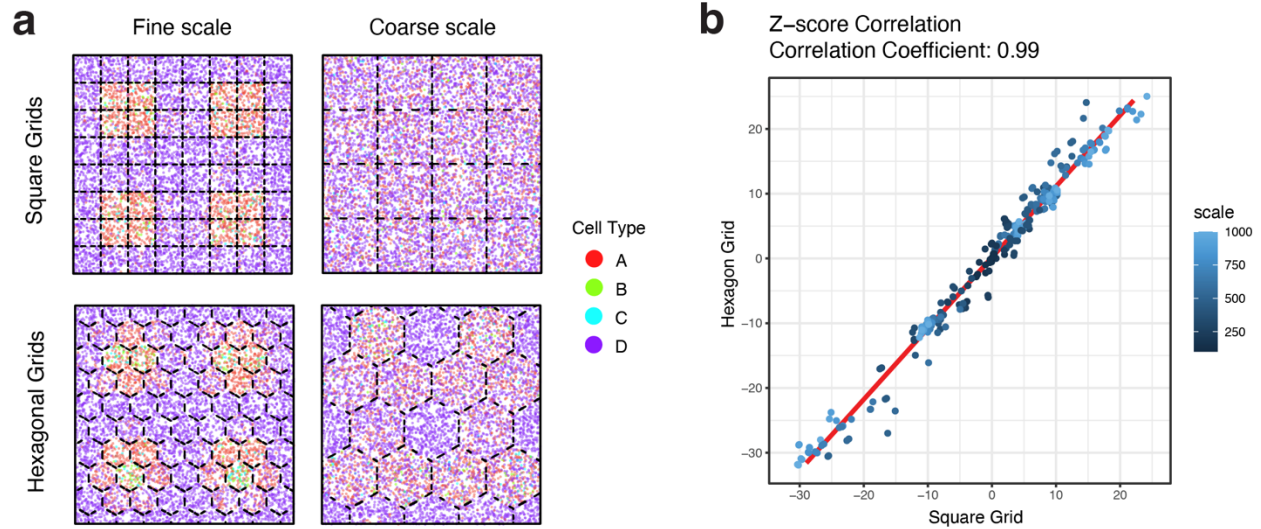
Supplementary Figure 7. Spatial visualization of selected cell types in the spleen samples. **a.** Visualization of Neutrophils/Monocytes and Podoplanin-enriched cells, exemplifying cell-type spatial relationship patterns consistent across all samples. **b.** Visualization of Ki67 and Follicular B cells, exemplifying cell-type spatial relationship patterns consistent across patients. **c.** Visualization of Blood endothelial and Follicular B cells, exemplifying non consistent cell-type spatial relationship patterns. Scale bars correspond to 250μm.
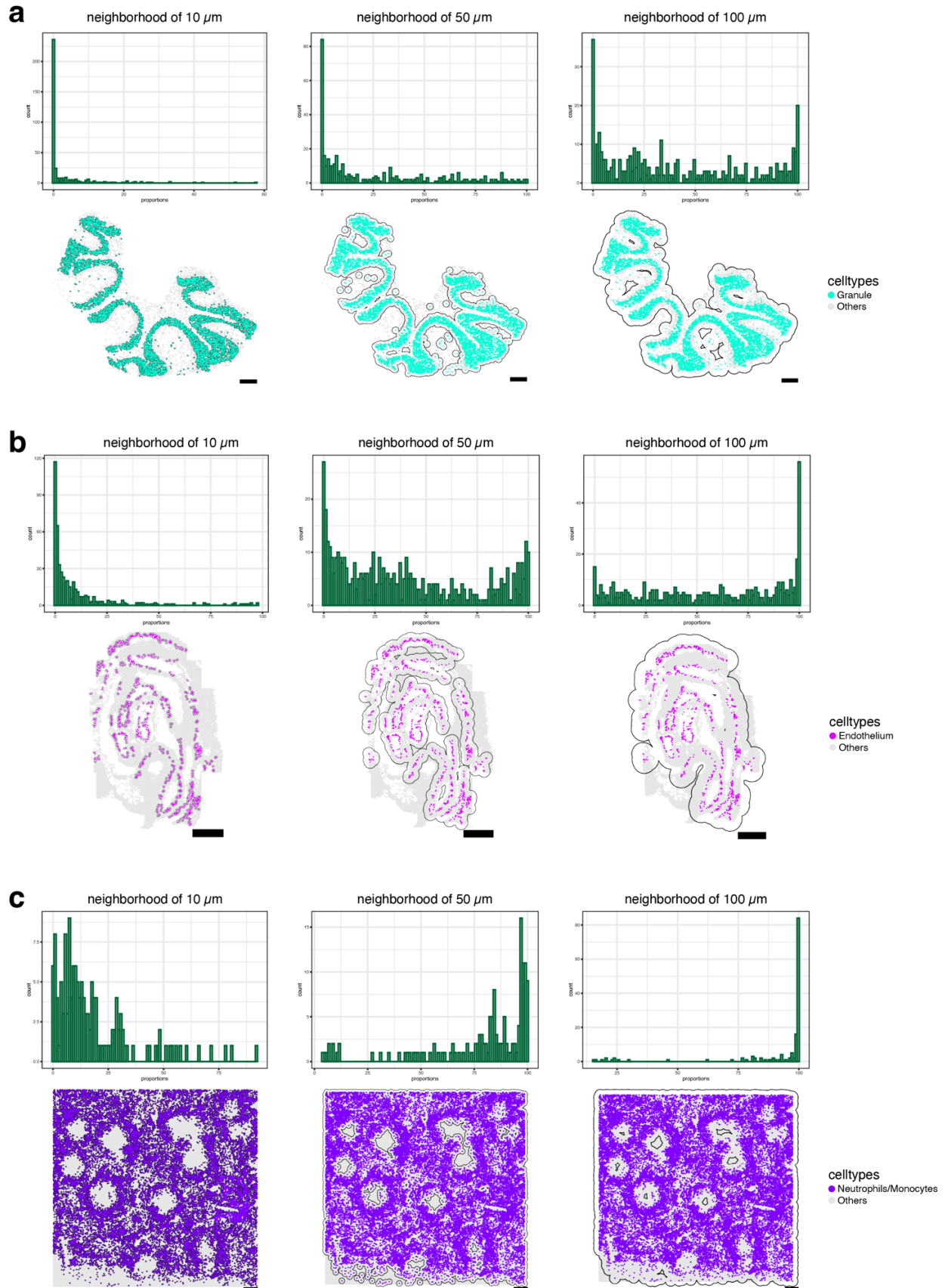
Supplementary Figure 8. The effects of the neighborhood size. **a-c**. Histogram of the cell-type proportion of cells from the neighbor of each cell type given neighborhood sizes of 10, 50 and 100 μm (top). Corresponding spatial visualization of the neighborhood as a black outline for chosen cell type (bottom). (**a**) Visualization of the cerebellum proportions and spatial visualization Granule neighborhoods. (**b**) Visualization of the embryo proportions and spatial visualization of the Endothelium neighborhoods. (**c**) Visualization of the PKHL spleen proportions and spatial visualization of the Neutrophils/Monocytes neighborhoods. Scale bars correspond to 250μm.

Supplementary Figure 9. **a**. Visualization of the shuffled labels using the square and hexagonal grid tiles on simulated dataset for finer and coarser scales. **b**. Consistency of Z-scores and scales for the different grid tile shapes. The x-axis represents the Z-score obtained using the square grid tiles and the y-axis represents the Z-score obtained using the hexagon grid tiles. The color saturation represents the scale in which the value was obtained. The red line represents the correlation of the values.